Carbon-Supported High-Entropy Oxide Nanoparticles as Stable Electrocatalysts for Oxygen Reduction Reactions

Tangyuan Li, Yonggang Yao, Byung Hee Ko, Zhennan Huang, Qi Dong, Jinlong Gao, Wilson Chen, Jianguo Li, Shuke Li, Xizheng Wang, Reza Shahbazian-Yassar,* Feng Jiao,* and Liangbing Hu*

Nanoparticles supported on carbonaceous substrates are promising electrocatalysts. However, achieving good stability for the electrocatalysts during long-term operations while maintaining high activity remains a grand challenge. Herein, a highly stable and active electrocatalyst featuring high-entropy oxide (HEO) nanoparticles uniformly dispersed on commercial carbon black is reported, which is synthesized via rapid high-temperature heating (≈1 s, 1400 K). Notably, the HEO nanoparticles with a record-high entropy are composed of ten metal elements (i.e., Hf, Zr, La, V, Ce, Ti, Nd, Gd, Y, and Pd). The rapid high-temperature synthesis can tailor structural stability and avoid nanoparticle detachment or agglomeration. Meanwhile, the high-entropy design can enhance chemical stability to prevent elemental segregation. Using oxygen reduction reaction as a model, the 10-element HEO exhibits good activity and greatly enhances stability (i.e., 92% and 86% retention after 12 and 100 h, respectively) compared to the commercial Pd/C electrocatalyst (i.e., 76% retention after 12 h). This superior performance is attributed to the high-entropy compositional design and synthetic approach, which offers an entropy stabilization effect and strong interfacial bonding between the nanoparticles and carbon substrate. The approach promises a viable route toward synthesizing carbon-supported high-entropy electrocatalysts with good stability and high activity for various applications.

1. Introduction

Carbon-supported nanoparticles are a family of efficient and cost-effective electrocatalysts that are widely used in electrochemical energy conversion and storage devices, such as fuel cells, electrolyzers, and metal–air batteries.[1–3] In general, good activity of the electrocatalysts is critical to achieve low overpotentials and thus high efficiency, meanwhile the stability also needs to be high to ensure long-term operations.[4] For carbon-supported nanoparticles, metals or metal oxides often serve as the active sites to provide desired catalytic activity, meanwhile carbon substrate usually acts as the support to anchor and disperse the nanoparticles.[5–8] Although significant efforts have been made to tailor the activity and stability simultaneously, achieving stable and active catalytic performance for long-term operations remains an outstanding challenge to the electrocatalysis community.[9–13] In particular, the electrocatalysts usually suffer from structural deformation, amorphization, and elemental segregation due to the interaction with reactive intermediates (e.g., *O, *OH, and *OOH), resulting in gradual decay of the catalytic activity.[14,15] Moreover, most carbon-supported nanoparticles exhibit weak interfacial bonding between the nanoparticles and carbon substrate, leading to performance deterioration as a result of nanoparticle detachment and/or agglomeration (**Figure 1**a).[16–19]

Recently, high-entropy oxide (HEO), which is composed of four or more metal cations with equimolar or near-equimolar

Dr. T. Li, Dr. Y. Yao, Dr. Q. Dong, J. Gao, Dr. J. Li, S. Li, Dr. X. Wang,
Prof. L. Hu
Department of Materials Science and Engineering
University of Maryland
College Park, MD 20742, USA
E-mail: binghu@umd.edu

B. H. Ko, W. Chen, Prof. F. Jiao
Center for Catalytic Science and Technology
Department of Chemical and Biomolecular Engineering
University of Delaware
Newark, DE 19716, USA
E-mail: jiao@udel.edu

Dr. Z. Huang, Prof. R. Shahbazian-Yassar
Department of Mechanical and Industrial Engineering
University of Illinois at Chicago
Chicago, IL 60607, USA
E-mail: rsyassar@uic.edu

Prof. L. Hu
Center for Materials Innovation
University of Maryland
College Park, MD 20742, USA

**ADVANCED
SCIENCE NEWS**
www.advancedsciencenews.com

**ADVANCED
FUNCTIONAL
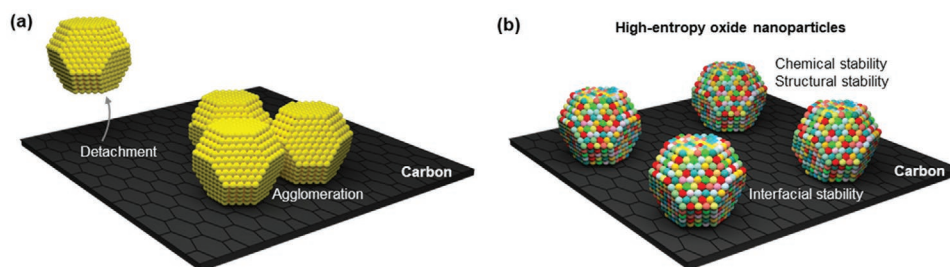MATERIALS**
www.afm-journal.de

Figure 1. Carbon-supported high-entropy oxide (HEO) nanoparticles as stable electrocatalysts. a) Conventional electrocatalysts often suffer from performance degradation during long-term operations as a result of nanoparticle detachment and agglomeration. b) A new family of stable electrocatalysts, composed by carbon-supported HEO nanoparticles, offers good activity and excellent structural, chemical as well as interfacial stabilities, enabled by the far-equilibrium synthetic approach (≈1400 K, ≈1 s) and high-entropy design.

concentrations in a single phase, has emerged as a promising candidate for electrocatalysis with improved chemical and structural stability due to the entropy stabilization effect.[20–24] In addition, HEOs with a tunable and broad compositional space have shown good performance in catalysis applications.[25] The mixed cationic sites can effectively interact with various intermediate species in electrocatalysis, resulting in good catalytic activity. However, the synthesis of HEO requires high temperature to ensure homogenous mixing of multiple elements with vastly different atomic radii, valences, and oxidation potentials,[24] which is challenging to be coupled with carbon substrate. This is because conventional high-temperature treatment with a prolonged furnace heating (e.g., hours) will result in severe particle agglomeration and carbothermal reduction of the oxide ($C + 2/x MO_x = 2/x M + CO_2\uparrow$, where M represents the metal element).[26,27] As carbon is indispensably used in electrochemical energy conversion and storage devices, it is critical to develop new synthetic strategies of carbon-supported HEO nanoparticles for electrocatalysis applications.

Herein, we report the synthesis of HEO nanoparticles (≈7 nm) uniformly dispersed on a commercial carbon powder substrate (Figure 1b), which possesses good activity and excellent stability as electrocatalysts. Our synthetic method features a far-equilibrium synthesis (≈1400 K, ≈1 s) enabled by electrical Joule heating of carbon materials. The high temperature (≈1400 K) ensures multi-elemental mixing to form a uniform HEO structure, and most importantly strengthens the interfacial bonding between the HEO nanoparticles and carbon substrate to improve the structural stability of the electrocatalyst. The high-entropy design reduces undesired elemental segregation processes, thereby enhancing the chemical stability of the electrocatalyst. In addition, the short thermal treatment time (≈1 s) is also critical to avoid nanoparticle agglomeration as well as carbothermal reduction of HEO during synthesis. Compared with literature reports (Figure S1, Supporting Information),[28–32] our synthesis temperature is among the highest while the duration is among the shortest, demonstrating a far-equilibrium process.[33] When tested in a model oxygen reduction reaction (ORR), the carbon-supported HEO nanoparticles containing up to 10 metal cations with a record-high entropy (Figure S2, Supporting Information) showed good catalytic activity and significantly improved stability compared to the commercial Pd/C electrocatalyst. Our approach largely broadens the compositional space of HEOs for material design, property optimization, catalyst discovery, and a range of applications.

2. Results and Discussion

Figure 2a schematically demonstrates the synthesis of carbon-supported HEO nanoparticles using our rapid high-temperature heating process. In a typical experiment, a precursor solution (0.025 mol L^{-1}) with various salts in equimolar ratio was mixed with carbon black using a targeted loading (e.g., 20 wt%). After drying, the mixture was evenly spread on a carbon paper heating element for radiative Joule heating. When a transient current was applied to the carbon paper (Figure S3, Supporting Information), the paper was instantly heated up to 1400 K within 0.4 s in air (Figure 2b). Homogenous HEO nanoparticles with single-phase structure were then synthesized on the surface of carbon black with uniform nanoparticle and elemental distributions. The high heating temperature and short heating time play key roles for the successful formation of well-dispersed and uniformly mixed HEO nanoparticles. In comparison to the conventional synthesis methods that employ mild temperatures (e.g., 873 K) and long heating time (≈2 h), the high temperature (≈1400 K) by our method effectively promotes multi-elemental mixing. In addition, the short heating time (≈1 s) prevents the undesired reduction of cations to metallic states, meanwhile avoiding nanoparticle agglomeration.

In a control experiment, we used conventional furnace heating method (1073 K in Ar for 2 h) to synthesize $(Cu,Ni,Co,Fe,Mn)_3O_{4-x}$ (x represents oxygen vacancy) nanoparticles on carbon black. The X-ray diffraction (XRD) and transmission electron microscopy (TEM) analyses demonstrate undesired oxide reduction (Figure 2c) and particle agglomeration (Figure 2d). We also used furnace heating to synthesize the $(Cu,Ni,Co,Fe,Mn)_3O_{4-x}$ nanoparticles on carbon black in air at 573 K for 2 h, while the sample was absent of single-phase structure (Figure S4, Supporting Information). In stark contrast, our rapid high-temperature synthesis allows for the formation of single-phase spinel $(Cu,Ni,Co,Fe,Mn)_3O_{4-x}$ nanoparticles (≈9 nm) uniformly dispersed on carbon black where the short heating time plays a critical role for avoiding nanoparticle agglomeration, as confirmed by XRD data (Figure 2c) and TEM studies (Figure 2e). High resolution TEM and elemental mapping of $(Cu,Ni,Co,Fe,Mn)_3O_{4-x}$ nanoparticles also demonstrate
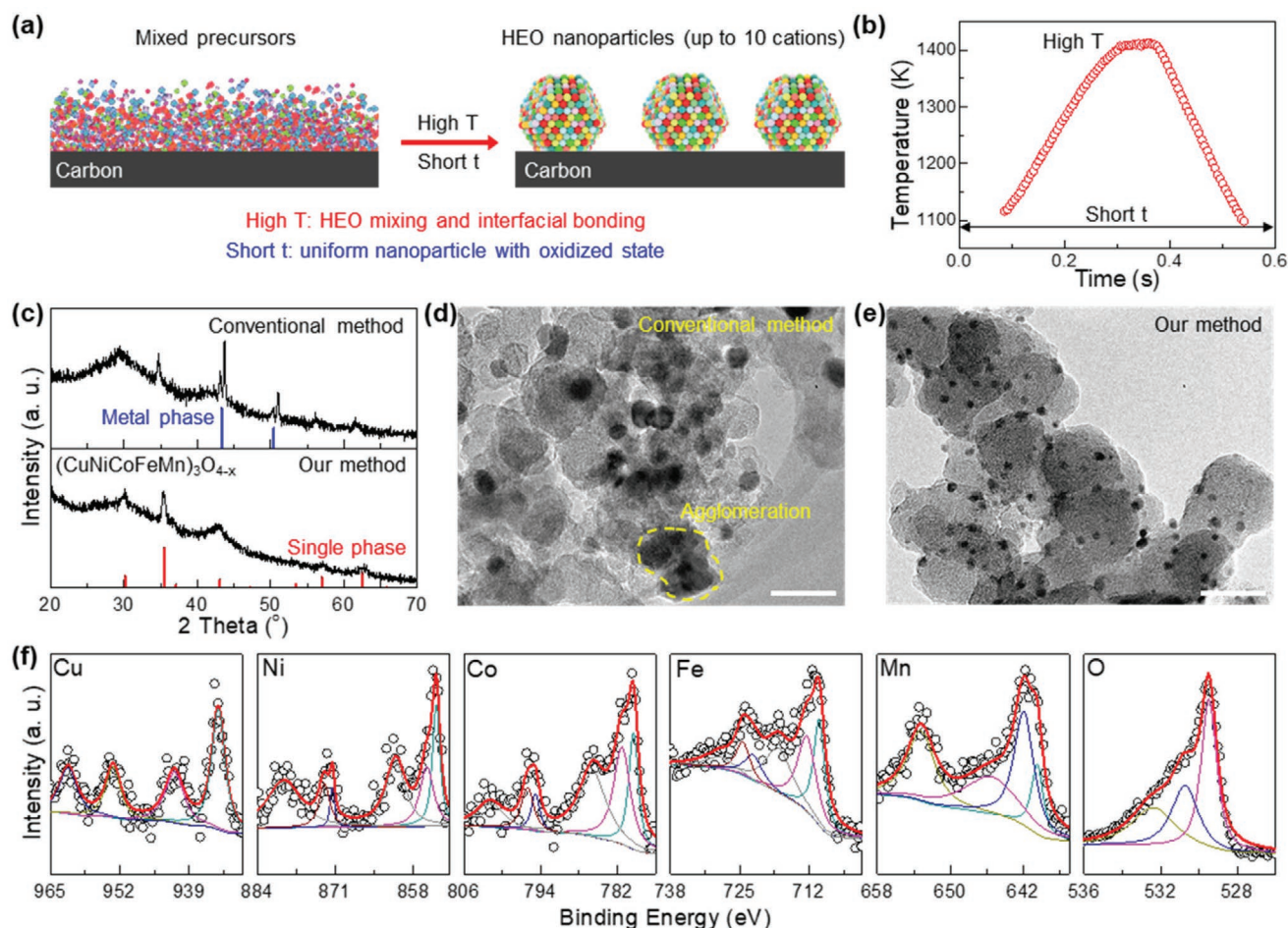
Figure 2. The synthesis of carbon-supported HEO nanoparticles using our rapid high-temperature method. a) Schematic for the synthesis of HEO nanoparticles supported on carbon substrate. b) The temperature profile used in the synthesis, which features high temperature and short heating time. c) XRD patterns of the $(Cu,Ni,Co,Fe,Mn)_3O_{4-x}$ synthesized by conventional furnace heating (1073 K in Ar for 2 h) and our rapid high-temperature method. d,e) TEM images of the $(Cu,Ni,Co,Fe,Mn)_3O_{4-x}$ synthesized by conventional furnace heating and our rapid high-temperature method. Scale bar: 50 nm. f) XPS spectra of Cu 2p, Ni 2p, Co 2p, Fe 2p, Mn 2p, and O 1s of the $(Cu,Ni,Co,Fe,Mn)_3O_{4-x}$ nanoparticles synthesized by our rapid high-temperature method, showcasing the cationic states of all the metal elements.

the spinel phase and the homogenous distribution of all the elements (Figure S5, Supporting Information). Moreover, X-ray photoelectron spectroscopy (XPS) spectra confirm that all cationic elements are in the oxidized states without any metallic components (Figure 2f). For example, the deconvoluted spectrum of Cu 2p (i.e., Cu $2p_{3/2}$ peak at 934 eV and Cu $2p_{1/2}$ at 954 eV) indicates that Cu was in 2+ valence state. Other XPS spectra also reveal the presence of Ni^{2+}, Ni^{3+}, Co^{2+}, Co^{3+}, Fe^{2+}, Fe^{3+}, Mn^{2+}, and Mn^{3+}. In addition, the O 1s spectrum was deconvoluted into three components, which represent the lattice oxygen bound to cations, oxygen vacancies, and chemisorbed oxygen species, respectively.[34] Note that the oxygen defects caused by hetero-valence element mixing in the HEO nanoparticles are desired for electrocatalysis such as ORR, as they can potentially serve as active sites to interact with the oxygen-containing intermediates.[15]

In the high-entropy system of $(Cu,Ni,Co,Fe,Mn)_3O_{4-x}$, five cationic elements possess various cation radii (e.g., 0.73 Å of Cu^{2+}, 0.63 Å of Fe^{3+}), crystalline structures for their corresponding unary oxides (e.g., tenorite for CuO, spinel for Fe_3O_4),

and oxidation potentials predicted by the Ellingham diagram (the sequence of oxidation potentials is Mn > Fe > Co > Ni > Cu, Figure S6, Supporting Information).[35,36] Our method can readily handle these drastically different physiochemical properties to incorporate all five elements into a single phase. This unique feat is benefited from the high temperature (≈1400 K), the rapid heating and quenching (heating duration of ≈1 s, quenching rate of ≈10^4 K s^{-1}) as well as high-entropy design. Note that in addition to the HEO formation, the short heating time also mitigates the reaction between carbon substrate and oxygen from air, which is critical to provide an oxidative environment while ensuring the integrity of carbon substrate. Enabled by our synthesis, we prepared a series of single-phase HEO nanoparticles supported on carbon black at gram-scale that have never been achieved before (Figure S7, Supporting Information), demonstrating the broad applicability and scalability of our approach.

The synthesis method allows us to prepare carbon-supported HEO nanoparticles with broad compositional options for specific reaction schemes. Note the HEO nanoparticles as the
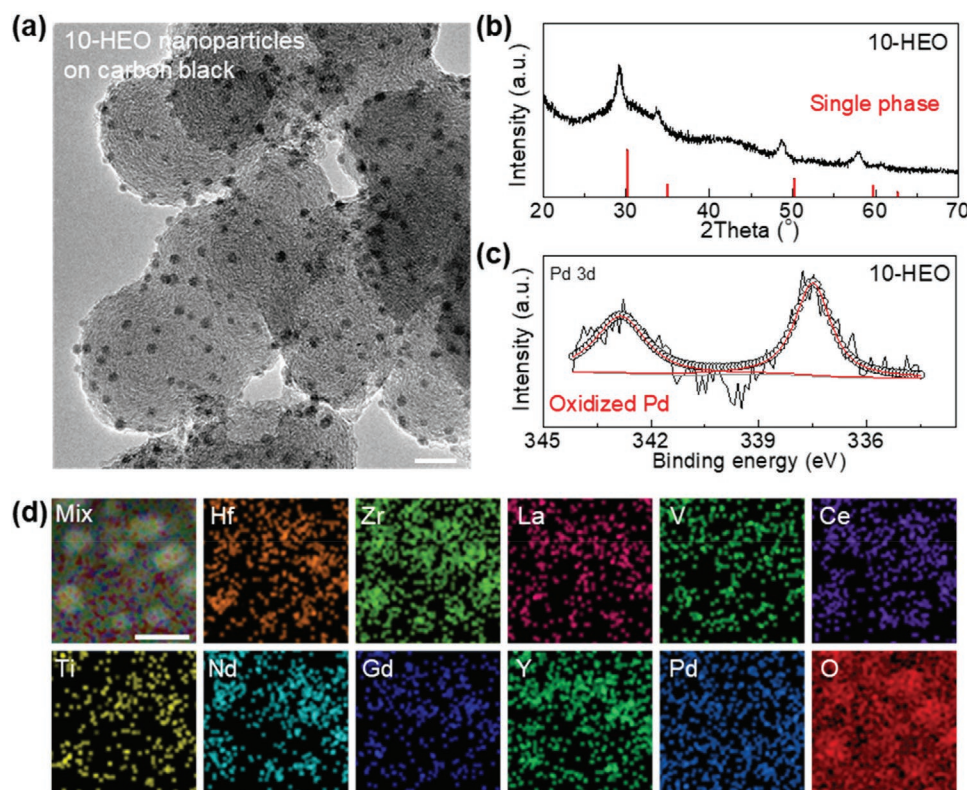
ADVANCED
SCIENCE NEWS
www.advancedsciencenews.com

ADVANCED
FUNCTIONAL
MATERIALS
www.afm-journal.de

Figure 3. Carbon-supported 10-HEO nanoparticles with record-high entropy. a) TEM image of the $(Hf,Zr,La,V,Ce,Ti,Nd,Gd,Y,Pd)O_{2-x}$ nanoparticles supported on the commercial carbon black substrate, showing uniform dispersion and nanoparticle size (≈7 nm). Scale bar: 20 nm. b) XRD of 10-HEO nanoparticles supported on the carbon black substrate, confirming a single-phase fluorite structure indexed to ZrO_2 (PDF#49-1642). c) XPS Pd 3d spectra of the 10-HEO nanoparticles, implying the oxidized state of Pd. d) Elemental mapping of the 10-HEO nanoparticles, demonstrating uniform mixing of all the elements. Scale bar: 10 nm.

electrocatalysts offer several advantages over the conventional noble metal-based electrocatalysts. First, the high-entropy nature and our high-temperature synthetic method ensure chemical and structural stability of the carbon-supported HEO nanoparticles. Second, the multi-elemental design of HEO readily reduces the cost due to the addition of non-noble elements to reduce the loading of noble metals. Third, as the active noble metal elements are diluted in the solid solution of HEO and also interact with other elements, the catalytic activity can be potentially benefited from the synergistic effect with better atom utilization efficiency.

We chose ORR as a model reaction and synthesized 10-element $(Hf,Zr,La,V,Ce,Ti,Nd,Gd,Y,Pd)O_{2-x}$ (10-HEO) nanoparticles with record-high entropy. The 10-HEO nanoparticles exhibit ultrafine structure (≈7 nm), which are uniformly dispersed on the commercial carbon black substrate (**Figure 3**a). The 10-HEO also shows single-phase fluorite structure and homogenous mixing among all the cationic metal elements, as revealed by XRD (Figure 3b), XPS (Figure 3c), and elemental mapping (Figure 3d). Notably, some elements in the 10-HEO such as Pd can be easily reduced to its metallic state due to the carbothermal reduction reaction according to the Ellingham diagram (Figure S6, Supporting Information).[35] Our control experiment on the synthesis of nanoparticles based on single-element Pd agrees with this prediction (Figure S8, Supporting Information). In contrast, the increased system entropy through

our high temperature synthesis decreases the formation Gibbs free energy of the HEO, leading to the stabilization of cationic species. The rapid (≈1 s) far-equilibrium synthesis also prevents the oxidized elements in the 10-HEO nanoparticles from being reduced to the metallic state by carbon. Considering the noble metal active sites are highly dispersed in the 10-HEO due to the presence of other cations, we expected the catalytic activity of the 10-HEO to be enhanced due to potential synergistic effect and better utilization of active sites. Importantly, the high-entropy nature and the strong interfacial bonding will offer desired stability for the carbon-supported 10-HEO nanoparticles in electrochemical reactions.

Using ORR as a model reaction, we tested the carbon-supported 10-HEO nanoparticles as an electrocatalyst (**Figure 4**a).[37,38] In the 10-HEO, Pd serves the major active site for the reaction, while the incorporation of other elements potentially offers synergistic effect and entropy stabilization for better catalytic activity and stability. Figure 4b shows the linear sweep voltammetry (LSV) curves of the commercial 5 wt% Pd/C, 22 wt% Pd, 22 wt% PdO, and 22 wt% 10-HEO nanoparticles supported on carbon black (i.e., Commercial Pd/C, Pd/C, PdO/C, and 10-HEO/C). The Pd/C electrocatalyst showed a half-wave potential ($E_{1/2}$) at 0.82 V versus reversible hydrogen electrode (RHE; unless further noted, the voltage in this work is normalized to RHE), which is slightly lower than those of the PdO/C (0.83 V) and 10-HEO/C (0.85 V) electrocatalysts.
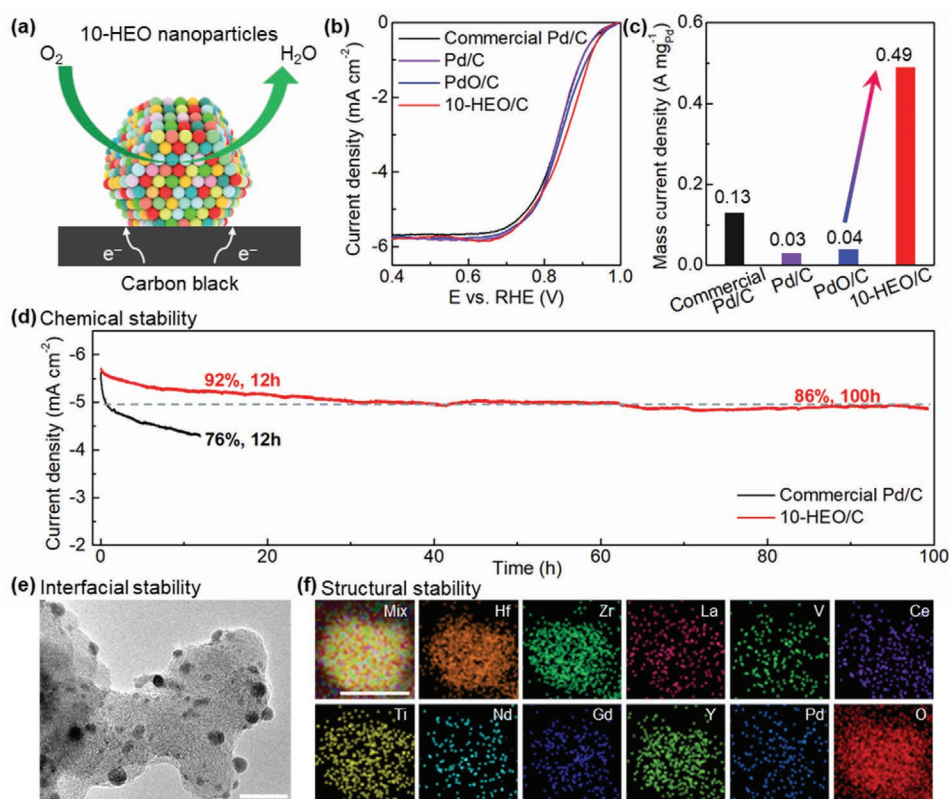
Figure 4. 10-HEO nanoparticles on carbon black as stable ORR electrocatalysts. a) Schematic of the 10-HEO nanoparticles dispersed on carbon black as ORR electrocatalysts. b) LSV curves of the commercial 5 wt% Pd/C, 22 wt% Pd, 22 wt% PdO, and 22 wt% 10-HEO nanoparticles dispersed on carbon black (i.e., Commercial Pd/C, Pd/C, PdO/C, and 10-HEO/C), tested in an O_2-saturated 0.1 M KOH electrolyte using a scan rate of 20 mV s^{-1} and a rotation rate of 1600 rpm. c) Current densities normalized by the mass of Pd for the commercial Pd/C, Pd/C, PdO/C, and 10-HEO/C, collected at 0.85 V versus RHE. d) Chronoamperometric profiles (i.e., percentage of current retention as a function of time) of the commercial Pd/C and the 10-HEO/C, tested in an O_2-saturated 0.1 M KOH electrolyte using a constant potential of 0.60 V versus RHE and 1600 rpm. e,f) TEM image (e, scale bar: 20 nm) and elemental mapping (f, scale bar: 5 nm) of the 10-HEO/C after the chronoamperometry test.

Cationic Pd appeared to be more active in ORR, which is in good agreement with previous studies.[39] The gravimetric current density of the 10-HEO/C is 0.49 A mg$_{Pd}^{-1}$ (normalized to Pd, Figure S9, Supporting Information) at 0.85 V, which is more than twelve times higher than that of the Pd/C (0.03 A mg$_{Pd}^{-1}$) or the PdO/C (0.04 A mg$_{Pd}^{-1}$), as shown in Figure 4c. The ORR performance of the 10-HEO/C also outperforms that of the commercial Pd/C with an $E_{1/2}$ at 0.82 V and a gravimetric current density of 0.13 A mg$_{Pd}^{-1}$ at 0.85 V. Note that our (Hf,Zr,La,V,Ce,Ti,Nd,Gd,Y)O$_{2-x}$ (9-HEO) nanoparticles without Pd show minimal ORR activity (Figure S10, Supporting Information), indicating that Pd is the major active site while the role of the other 9 elements in the 10-HEO is to stabilize Pd into the single-phase oxide matrix. As Pd is well-distributed in the 10-HEO, the enhanced performance of the 10-HEO/C electrocatalyst may also be attributed to the unsaturated surface of the cationic Pd atoms, similar to the single-atom cases.[40] In addition, owing to the mixing of multiple elements with different valence, the 10-HEO possesses oxygen defects compared to the single-element PdO. We hypothesize that the presence of oxygen vacancies also contributes to the enhanced ORR activity. In other words, in addition to the synergistic effect of Pd and other elements, the oxidation state of Pd and the

presence of oxygen defects in the 10-HEO also contribute to the enhanced ORR activity. We also measure the ORR performance of the 10-HEO/C at various rotation speed during LSV scans (Figure S11, Supporting Information). The Koutecky-Levich plot indicates a 4e$^-$ mechanism, which is desired for high energy density fuel cell applications.

The chemical stability of the 10-HEO/C was evaluated by cyclic voltammetry and chronoamperometry. We employed accelerated cyclic voltammetry (scanning between 0.6 and 1.0 V at 50 mV s^{-1}) to evaluate the durability of the 10-HEO/C. The LSV curves of the 10-HEO/C before and after cycling almost overlap with each other, together demonstrating an $E_{1/2}$ at 0.85 V (Figure S12, Supporting Information). During the chronoamperometry test, the 10-HEO/C electrocatalyst maintained 86% of its initial current after 100 h operation, while the commercial Pd/C suffered a quick loss of activity by 24% only after 12 h (92% retention for 10-HEO/C electrocatalyst after 12 h) (Figure 4d). Post analysis revealed that a weak interaction between Pd and carbon substrate in the commercial Pd/C led to the migration and agglomeration of Pd particles (Figure S13, Supporting Information), which caused substantial activity loss. In comparison, the 10-HEO/C electrocatalyst still maintained the uniform nanoparticle dispersion on the commercial carbon

substrate with homogenous elemental distribution after 100 h of operation (Figure 4e,f), showcasing excellent structural and interfacial stabilities. The stable and high catalytic activity of the 10-HEO/C sample up to 100 h is one of the best combinations compared to the state-of-the-art electrocatalysts (Table S1, Supporting Information).[18,29,41–43] These results suggest that the carbon-supported HEO nanoparticles hold great promise as highly active and stable electrocatalysts for practical electrochemical applications.

3. Conclusion

In summary, we developed a series of HEO nanoparticles uniformly supported on commercial carbon powder substrates through a far-equilibrium synthesis method (i.e., rapid high-temperature heating), which significantly expanded the compositional space of carbon-supported electrocatalysts. The high-temperature synthesis and high-entropy design enable the uniform mixing of multiple elements with vastly different physicochemical properties into a single phase. The ultrafast heating time avoids undesired oxide reduction and nanoparticle agglomeration, and thus resulted in the uniform dispersion of the HEO nanoparticles. Such a process ensures good structural stability owing to the strengthened interfacial bonding between nanoparticles and substrate, as well as enhanced chemical stability due to the entropy-stabilization effect to prevent elemental segregation. The newly developed 10-HEO/C electrocatalyst showed high activity and most importantly superior stability for ORR (92% and 86% retention after 12 and 100 h, respectively) compared to the commercial Pd/C (76% retention after 12 h). This work provides a new route toward synthesizing a range of high-entropy nanoparticles supported on carbon substrates as highly stable and active electrocatalysts.

4. Experimental Section

Material Preparation: Commercial carbon black (Vulcan XC72, Cabot) was chosen as the substrate to support HEO nanoparticles. The commercial 5.0 wt% Pd/C was purchased from Sigma Aldrich. The used chemicals include nitrates (i.e., $CoN_2O_6 \cdot 6H_2O$, $FeN_3O_9 \cdot 9H_2O$, $CuN_2O_6 \cdot 6H_2O$, $NiN_2O_6 \cdot 6H_2O$, $MnN_2O_6 \cdot 4H_2O$, $LaN_3O_9 \cdot 6H_2O$, $CeN_3O_9 \cdot 6H_2O$, $YN_3O_9 \cdot 6H_2O$, $GdN_3O_9 \cdot 6H_2O$, and $NdN_3O_9 \cdot 6H_2O$) and chlorides (i.e., $TiCl_4$, $ZrCl_4$, VCl_3, $HfCl_4$, and $PdCl_2$) purchased from Sigma Aldrich. The precursor solution (0.025 mol L^{-1}) was prepared by dissolving various salts (having equimolar concentration) in ethanol. The mixed solution was added into carbon black with a targeted loading concentration, and then sonicated for 120 min. The mixed precursors were freeze-dried prior to the HEO synthesis. The obtained powders were evenly spread on commercial carbon paper (AvCarb MGL370, FuelCellStore) which was fixed to copper tapes supported by alumina ceramic sheets. The carbon paper was connected to a DC power supply (MP10050D, StarPower), and then heated under air by thermal shock to provide the heating source for the HEO synthesis. The mixed powders were rapidly heated by the radiative heating ($\approx$1400 K, $\approx$1 s), and thus the HEO nanoparticles were synthesized, and uniformly dispersed on carbon black substrate. The 22 wt% Pd/C was synthesized by the radiative heating method (Figure S14a, Supporting Information). The 22 wt% PdO/C was synthesized using an impregnation approach, where the precursor solution was prepared by dissolving $Pd(NO_3)_2 \cdot nH_2O$ in mixed ethanol and dilute nitric acid, and then the solution was mixed with carbon black powder. The resultant mixture was sonicated for 120 min, and then was freeze-dried. The resultant powder was heated at 623 K for 2 h under air in a tube furnace (Figure S14b, Supporting Information).

Characterization: Temperature measurement of the carbon paper during the synthesis was evaluated by a high-speed camera (Vision Research Phantom v12.0) based on the black-body radiation mechanism. A diffractometer (D8 Advance, Bruker, Karlsruhe, Germany) was used with Cu Kα radiation to characterize XRD spectra of the oxide nanoparticles on carbon black at room temperature. The mass loading of oxide nanoparticles was collected by thermogravimetric analysis (Discovery SDT 650, TA Instruments). An AXIS 165 spectrometer (Kratos, Manchester, UK) was used to determine XPS spectra of oxide nanoparticles. Transmission electron microscopy (TEM; JEM-2100, JEOL, Tokyo, Japan) and STEM (JEM-ARM200F, JEOL, Tokyo, Japan) were used to reveal the microstructures of oxide nanoparticles, and their elemental mappings were achieved using energy dispersive spectroscopy (EDS; X-Max^N-100TLE, Oxford Instruments, Oxford, UK).

Electrochemical Measurement: The carbon-supported HEO nanoparticles and commercial 5.0 wt% Pd/C as the ORR catalysts were tested. In order to prepare the catalyst ink for ORR test, 2 mg carbon-supported HEO nanoparticles or commercial Pd/C were dispersed in 400 µL mixed solutions of Nafion, water, and isopropanol (1:50:150), and then sonicated for 30 min. The as-prepared 15 µL ink was dropped onto the 0.196 cm^2 glassy carbon, and further dried at room temperature. The three-electrode system was used on an electrochemical workstation (VMP-300, Bio-Logic) with a rotator (Pine Instruments). The obtained film on the glassy carbon was used as the working electrode. The counter electrode was graphite, and the reference electrode was the Ag/AgCl (saturated KCl) electrode. Used electrolyte was 0.1 M KOH which was purged with O_2 for 20 min before each test, and subjected to O_2 flow under room temperature during the measurements. Accelerated cyclic voltammetry of 500 cycles was performed by scanning between 0.6 and 1.0 V versus RHE at 50 mV s^{-1}.

Supporting Information

Supporting Information is available from the Wiley Online Library or from the author.

Conflict of Interest

The authors declare no conflict of interest.

Author Contributions

T.L., Y.Y., B.H.K., Z.H., and Q.D. contributed equally to this work. L.H., T.L., and Y.Y. designed the experiments. T.L., Y.Y., Q.D., J.G., J.L., S.L., and X.W. conducted materials preparation and characterization. Z.H. and R.S.-Y. carried out the high-resolution microscopy. T.L., W.C., B.K., and F.J. performed the catalysis measurements. L.H. and T.L. wrote the paper. All authors commented to the final manuscript.

Data Availability Statement

Research data are not shared.

Keywords

electrocatalysts, high-entropy oxides, high-temperature synthesis, nanoparticles

[1] M. Shao, Q. Chang, J. P. Dodelet, R. Chenitz, *Chem. Rev.* **2016**, *116*, 3594.

[2] X. Ge, A. Sumboja, D. Wuu, T. An, B. Li, F. W. T. Goh, T. S. A. Hor, Y. Zong, Z. Liu, *ACS Catal.* **2015**, *5*, 4643.

[3] C. Wei, R. R. Rao, J. Peng, B. Huang, I. E. L. Stephens, M. Risch, Z. J. Xu, Y. Shao-Horn, *Adv. Mater.* **2019**, *31*, 1806296.

[4] X. Wang, A. Vasileff, Y. Jiao, Y. Zheng, S. Z. Qiao, *Adv. Mater.* **2019**, *31*, 1803625.

[5] M. Luo, Z. Zhao, Y. Zhang, Y. Sun, Y. Xing, F. Lv, Y. Yang, X. Zhang, S. Hwang, Y. Qin, J. Y. Ma, F. Lin, D. Su, G. Lu, S. Guo, *Nature* **2019**, *574*, 81.

[6] Y. Zhu, W. Zhou, Z. Shao, *Small* **2017**, *13*, 1603793.

[7] H. Sun, L. Mei, J. Liang, Z. Zhao, C. Lee, H. Fei, M. Ding, J. Lau, M. Li, C. Wang, X. Xu, G. Hao, B. Papandrea, I. Shakir, B. Dunn, Y. Huang, X. Duan, *Science* **2017**, *356*, 599.

[8] L. F. Chen, Y. Feng, H. W. Liang, Z. Y. Wu, S. H. Yu, *Adv. Energy Mater.* **2017**, *7*, 1700826.

[9] Y. Liang, Y. Li, H. Wang, J. Zhou, J. Wang, T. Regier, H. Dai, *Nat. Mater.* **2011**, *10*, 780.

[10] J. Suntivich, H. A. Gasteiger, N. Yabuuchi, H. Nakanishi, J. B. Goodenough, Y. Shao-Horn, *Nat. Chem.* **2011**, *3*, 546.

[11] Y. Zhao, L. Xu, L. Mai, C. Han, Q. An, X. Xu, X. Liu, Q. Zhang, *Proc. Natl. Acad. Sci. USA* **2012**, *109*, 19569.

[12] H. Tabassum, R. Zou, A. Mahmood, Z. Liang, Q. Wang, H. Zhang, S. Gao, C. Qu, W. Guo, S. Guo, *Adv. Mater.* **2018**, *30*, 1705441.

[13] H. Zhu, S. Zhang, Y. X. Huang, L. Wu, S. Sun, *Nano Lett.* **2013**, *13*, 2947.

[14] H. Osgood, S. V. Devaguptapu, H. Xu, J. Cho, G. Wu, *Nano Today* **2016**, *11*, 601.

[15] W. T. Hong, M. Risch, K. A. Stoerzinger, A. Grimaud, J. Suntivich, Y. Shao-Horn, *Energy Environ. Sci.* **2015**, *8*, 1404.

[16] J. Suntivich, H. A. Gasteiger, N. Yabuuchi, Y. Shao-Horn, *J. Electrochem. Soc.* **2010**, *157*, B1263.

[17] Y. Liang, H. Wang, P. Diao, W. Chang, G. Hong, Y. Li, M. Gong, L. Xie, J. Zhou, J. Wang, T. Z. Regier, F. Wei, H. Dai, *J. Am. Chem. Soc.* **2012**, *134*, 15849.

[18] Y. Liang, H. Wang, J. Zhou, Y. Li, J. Wang, T. Regier, H. Dai, *J. Am. Chem. Soc.* **2012**, *134*, 3517.

[19] Y. Tan, C. Xu, G. Chen, X. Fang, N. Zheng, Q. Xie, *Adv. Funct. Mater.* **2012**, *22*, 4584.

[20] C. M. Rost, E. Sachet, T. Borman, A. Moballegh, E. C. Dickey, D. Hou, J. L. Jones, S. Curtarolo, J. P. Maria, *Nat. Commun.* **2015**, *6*, 8485.

[21] S. Jiang, T. Hu, J. Gild, N. Zhou, J. Nie, M. Qin, T. Harrington, K. Vecchio, J. Luo, *Scr. Mater.* **2018**, *142*, 116.

[22] A. Sarkar, Q. Wang, A. Schiele, M. R. Chellali, S. S. Bhattacharya, D. Wang, T. Brezesinski, H. Hahn, L. Velasco, B. Breitung, *Adv. Mater.* **2019**, *31*, 1806236.

[23] F. Okejiri, Z. Zhang, J. Liu, M. Liu, S. Yang, S. Dai, *ChemSusChem* **2020**, *13*, 111.

[24] C. Oses, C. Toher, S. Curtarolo, *Nat. Rev. Mater.* **2020**, *5*, 295.

[25] T. Li, Y. Yao, Z. Huang, P. Xie, Z. Liu, M. Yang, J. Gao, K. Zeng, A. H. Brozena, G. Pastel, M. Jiao, Q. Dong, J. Dai, S. Li, H. Zong, M. Chi, J. Luo, Y. Mo, G. Wang, C. Wang, R. Shahbazian-yassar, L. Hu, *Nat. Catal.* **2021**, *4*, 62.

[26] A. Aijaz, J. Masa, C. Rösler, W. Xia, P. Weide, A. J. R. Botz, R. A. Fischer, W. Schuhmann, M. Muhler, *Angew. Chem., Int. Ed.* **2016**, *55*, 4087.

[27] H. Zhu, L. Gu, D. Yu, Y. Sun, M. Wan, M. Zhang, L. Wang, L. Wang, W. Wu, J. Yao, M. Du, S. Guo, *Energy Environ. Sci.* **2017**, *10*, 321.

[28] Z. S. Wu, S. Yang, Y. Sun, K. Parvez, X. Feng, K. Müllen, *J. Am. Chem. Soc.* **2012**, *134*, 9082.

[29] C. Li, X. Han, F. Cheng, Y. Hu, C. Chen, J. Chen, *Nat. Commun.* **2015**, *6*, 7345.

[30] T. Zhou, W. Xu, N. Zhang, Z. Du, C. Zhong, W. Yan, H. Ju, W. Chu, H. Jiang, C. Wu, Y. Xie, *Adv. Mater.* **2019**, *31*, 1807468.

[31] X. Zhou, Z. Dai, S. Liu, J. Bao, Y. G. Guo, *Adv. Mater.* **2014**, *26*, 3943.

[32] M. Wan, H. Zhu, S. G. Zhang, H. N. Jin, Y. K. Wen, L. N. Wang, M. Zhang, M. L. Du, *Electrochim. Acta* **2018**, *279*, 301.

[33] Y. Yao, Z. Huang, P. Xie, S. D. Lacey, R. J. Jacob, H. Xie, F. Chen, A. Nie, T. Pu, M. Rehwoldt, D. Yu, M. R. Zachariah, C. Wang, R. Shahbazian-Yassar, J. Li, L. Hu, *Science* **2018**, *359*, 1489.

[34] J. Bao, X. Zhang, B. Fan, J. Zhang, M. Zhou, W. Yang, X. Hu, H. Wang, B. Pan, Y. Xie, *Angew. Chem.* **2015**, *127*, 7507.

[35] T. B. Reed, *Free Energy of Formation of Binary Compounds*, MIT Press, Cambridge, MA **1971**.

[36] R. D. Shannon, *Acta Crystallogr., Sect. A: Found. Crystallogr.* **1976**, *32*, 751.

[37] Z. F. Huang, J. Song, Y. Du, S. Xi, S. Dou, J. M. V. Nsanzimana, C. Wang, Z. J. Xu, X. Wang, *Nat. Energy* **2019**, *4*, 329.

[38] X. F. Lu, B. Y. Xia, S. Zang, X. W. (David) Lou, *Angew. Chem.* **2019**, *59*, 4662.

[39] Y. Zhu, W. Zhou, Y. Chen, J. Yu, X. Xu, C. Su, M. O. Tadé, Z. Shao, *Chem. Mater.* **2015**, *27*, 3048.

[40] Y. Chen, S. Ji, C. Chen, Q. Peng, D. Wang, Y. Li, *Joule* **2018**, *2*, 1242.

[41] X. Yan, Y. Jia, J. Chen, Z. Zhu, X. Yao, *Adv. Mater.* **2016**, *28*, 8771.

[42] W. Wang, L. Kuai, W. Cao, M. Huttula, S. Ollikkala, T. Ahopelto, A. P. Honkanen, S. Huotari, M. Yu, B. Geng, *Angew. Chem., Int. Ed.* **2017**, *56*, 14977.

[43] T. Hu, Y. Wang, L. Zhang, T. Tang, H. Xiao, W. Chen, M. Zhao, J. Jia, H. Zhu, *Appl. Catal., B* **2019**, *243*, 175.